Circuit analysis of radiation reaction in metamaterials by retarded electromagnetic coupling

AUTHOR(S):

Nakata, Ryoma; Hisakado, Takashi; Matsushima, Tohlu; Wada, Osami

CITATION:

Nakata, Ryoma ...[et al]. Circuit analysis of radiation reaction in metamaterials by retarded electromagnetic coupling. IET Circuits, Devices & Systems 2022, 16(4): 311-321

ISSUE DATE:

2022-07

URL:

http://hdl.handle.net/2433/277479

Received: 7 May 2021 | Revised: 8 October 2021 | Accepted: 5 November 2021

IET Circuits, Devices & Systems

DOI: 10.1049/cds2.12104

The Institution of Engineering and Technology WILEY

ORIGINAL RESEARCH

Circuit analysis of radiation reaction in metamaterials by retarded electromagnetic coupling

Ryoma Nakata | **Takashi Hisakado** | **Tohlu Matsushima** | **Osami Wada**

Faculty of Engineering, Graduate School of Engineering, Kyoto University, Kyoto, Japan

Correspondence

Takashi Hisakado, Faculty of Engineering, Graduate School of Engineering, Kyoto University, Kyoto, Japan.
Email: hisakado.takashi.7x@kyoto-u.ac.jp

Funding information

Grants-in-Aid for Scientific Research, Grant/Award Numbers: 18K04139, 15K06063

Abstract

Because radiation is essential in high-frequency circuits, such as those used in metamaterials and plasmonics, the investigation of radiation loss is important. This study describes the characteristics of radiation loss, which is a radiation reaction in circuits with retarded electromagnetic couplings. The structure of wired metallic spheres is used to demonstrate metamaterial equivalent circuits, where charges and current exist on the spheres and wires, respectively. An inductance matrix and a potential coefficient matrix with retarded electromagnetic couplings are defined to address the radiation reaction. Subsequently, based on the topology of the wires and spheres, an equivalent circuit equation with retardation is formulated to discuss the losses in the resonant circuit caused by the inductive and capacitive elements. Thereafter, the relationship between the resonant frequency and radiation loss caused by the retarded couplings is demonstrated and the difference between the retarded couplings and couplings with transmission lines is clarified. Furthermore, we indicate that retarded coupling generates singularity on a dispersion curve for a one-dimensional array of resonant circuits. Thus, the circuit with retarded couplings generates novel characteristics of radiation reactions that are not represented by the circuit without retardation. This circuit analysis is expected to afford new aspects in studies on topics, such as metamaterials and plasmonics.

KEYWORDS

circuit analysis, metamaterial, radiation reaction, retarded coupling, transmission line

1 | INTRODUCTION

Equivalent circuit models are powerful tools for analysis and design of electromagnetic phenomena. Recently, the design and synthesis of electromagnetic properties in complex metallic structures were conducted for metamaterials and plasmonics. The effectiveness of the equivalent circuit models was reported [1–3]. Such equivalent circuit models can provide physical insight into resonance [4, 5], coupling [6], and propagation [7] in electromagnetic phenomena. However, the radiation loss caused by the radiation reaction is not easily described because the mechanism of the radiation loss is different from the ohmic loss [8–10], despite radiation being an important factor in high-frequency circuits.

To represent the radiation loss in the equivalent circuit, it is important to include the delay caused by the retarded potentials [11–13]. Hence, the radiation reaction is represented as feedback using retarded electromagnetic couplings. The partial element equivalent circuit (PEEC) is a full-wave circuit model with meshes of metallic structures [14–16], representing the radiation loss as the retardations between the meshes [17, 18]. Recently, the topic of the passivity of PEEC [19] and the discussion on its validity as a model of radiation has been reported in [20, 21]. Another method has been proposed to derive a simple circuit by specified structures, consisting of capacitive spheres and inductive wires [22]. In this structure, the topology of the wires corresponds to the topology of the circuit, which simplifies the design of the topology and the

radiation loss is modelled by retarded couplings [23]. Thus, lumped element circuits with retardation are essential for modelling the electromagnetic radiation losses.

The radiation reaction caused by the retarded electromagnetic couplings provides not only the radiation loss in the lumped circuit model but it also identifies other properties in the circuits. For example, the resonant frequencies are affected by the radiation reactions and the retarded couplings contribute to the relationship between the radiation loss and the resonant frequency [23]. Furthermore, the radiation reaction can alter the dispersion curves in the metamaterials [7, 24, 25]. Thus, it is important to clarify these properties of the radiation reaction using the equivalent circuit models with retarded couplings.

This study proposes the circuit analysis of the radiation reaction using a lumped element circuit with retarded couplings. To clarify the effects of the retardation, we use the wired metallic sphere structure [22] and consider the retarded inductive and capacitive couplings [23]. The validity of the models with retardation was confirmed in [23] through the comparison with electromagnetic simulations. However, because the derivation of the circuit equation was based on Green's function and the boundary condition on conductors, its relationship with Kirchhoff's law in ordinary circuit analysis is unclear. Therefore, in this study, we present the derivation of the circuit equation using Kirchhoff's law after the circuit elements are given. We used the potential coefficient matrix instead of the capacitance matrix to describe capacitive couplings because the charges generate the potential as given by Maxwell's equation. Based on the wire and sphere topologies, we formulate the circuit equation and the relationship with energy using Tellegen's theorem.

Next, we demonstrate the advantages of the circuit analysis with retardations over the conventional circuit without retardation. We discuss the losses caused by the retardation of the inductance and potential matrices using a simple resonator. The losses are explained by the rotation of impedance in a complex plane caused by the retardation. We show the relationship between the radiation loss and resonant frequency in coupled resonators and clarify the difference between the retarded coupling and transmission line couplings, which also provide coupling delays. Furthermore, we show the generation of the singularity on the dispersion curve with the one-dimensional (1-D) periodic array of resonators and explain the radiation loss discontinuity on the light line analytically.

In the circuit analysis of the radiation reaction, the main contributions of this work are fourfold: (1) proposing a power balance according to Tellegen's theorem in Section 2; (2) depicting the difference in the contribution of capacitive and inductive elements to radiation in Section 3; (3) describing the essential difference between the retarded coupling and delays in transmission line in Section 4; and (4) proving the singularity on a dispersion curve created by the retarded coupling in Section 5. Since this circuit analysis clearly describes the power balance including radiation reaction, the potential applications include the design of antennas with complex structures, wireless power transfer, and transmission lines that do not have explicit return paths.

2 | CIRCUIT EQUATION WITH RETARDED COUPLING

2.1 | Inductance matrix with retarded coupling

Inductances with retardation are represented by complex numbers in the frequency domain. We review an example of self-inductance with retardation using the metallic structure in Figure 1 [23]. Here, D is the length between the centres of the two spheres and the radii of the wire and spheres are denoted by a and b, respectively. Assuming that the current in the wire is uniform and $a \ll b \ll D$, the inductance of the wire is approximated as

$$L_s(\omega) = \frac{\mu_0}{4\pi}\int_b^{D-b}\int_0^D \frac{\cos\left(\omega\frac{\sqrt{(z-z')^2+a^2}}{c}\right)}{\sqrt{(z-z')^2+a^2}}\mathrm{d}z'\mathrm{d}z - \mathrm{j}\frac{\mu_0}{4\pi}\int_0^D\int_0^D \frac{\sin\left(\omega\frac{\sqrt{(z-z')^2+a^2}}{c}\right)}{\sqrt{(z-z')^2+a^2}}\mathrm{d}z'\mathrm{d}z, \tag{1}$$

where c is the light speed. The details of the derivation using Green's function in 3D with retardation is shown in [23]. The complex inductance is caused by the phase shift of

$$e^{-\mathrm{j}\omega\frac{\sqrt{(z-z')^2+a^2}}{c}}, \tag{2}$$

between the position z' of the current on the central axis of the wire and the position z of the estimated electric field on the surface of the wire. We consider this property of retardation in this study.

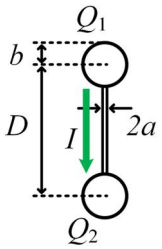

FIGURE 1 Structure of a resonator of a single meta-atom. The wires indicate the inductance and spheres indicate the potential coefficients. We use parameters a = 0.01 mm, b = 1 mm and D = 7 mm in this study

Mutual inductance with retardation, of the structure in Figure 2, can be approximated as

$$L_{12} = \frac{\mu_0}{4\pi}\int_0^D\int_0^D \frac{\exp\left(-\mathrm{j}\omega\frac{\sqrt{(z-z')^2+h^2}}{c}\right)}{\sqrt{(z-z')^2+h^2}}\mathrm{d}z'\mathrm{d}z \tag{3}$$

$$\simeq \frac{\mu_0 D}{2\pi}\left(\ln(\eta+\sqrt{1+\eta^2}) - \sqrt{1+\frac{1}{\eta^2}} + \frac{1}{\eta}\right)e^{-\mathrm{j}\omega\frac{h}{c}}, \tag{4}$$

where $\eta = D/h$ and the derivation is presented in [23]. The phase shift is caused by the distance h between the wires. If $\eta \ll 1$ is satisfied, the mutual inductance can be approximated as

$$L_{12} \sim \frac{\mu_0}{4\pi}\frac{D^2}{h}e^{-\mathrm{j}\omega\frac{h}{c}}. \tag{5}$$

and the mutual inductance has the factor $\frac{1}{h}e^{-\mathrm{j}\omega\frac{h}{c}}$, which corresponds to the Green's function in 3D with retardation. We present a circuit analysis of the properties of elements with this type of retarded coupling. If there are N inductive elements, such as wires, we can define $N \times N$ inductance matrix $\boldsymbol{L}$ by the retarded inductances.

2.2 | Potential coefficient matrix with retarded coupling

Because the charge contributes to the potential in Maxwell equations, we introduce potential coefficients instead of capacitances. First, the self-potential coefficient of a metallic sphere, shown in Figure 1, is represented as

$$P_{11} \simeq \frac{\exp\left(-\mathrm{j}\omega\frac{b}{c}\right)}{4\pi\varepsilon_0 b}, \tag{6}$$

[23]. Thus, the self-potential coefficient has a factor $\frac{1}{b}e^{-\mathrm{j}\omega\frac{b}{c}}$, which corresponds to the Green's function in 3D with retardation.

If $b \ll D$ is satisfied in Figure 1, the mutual potential coefficient P_{12} is represented as

$$P_{12} \simeq \frac{\exp\left(-\mathrm{j}\omega\frac{D}{c}\right)}{4\pi\varepsilon_0 D}. \tag{7}$$

and has the factor $\frac{1}{D}e^{-\mathrm{j}\omega\frac{D}{c}}$. If there are M capacitive elements such as spheres, we can define the $M \times M$ potential coefficient matrix $\boldsymbol{P}$ by the retarded potential coefficients.

Although we consider examples of the wired metallic spheres, an inductance matrix $\boldsymbol{L}$ and a potential coefficient matrix $\boldsymbol{P}$ can be defined for inductive elements of thin wire structures with uniform currents and capacitive elements of massive structures with uniform voltages based on the method in [23]. In this study, we present the circuit analysis by Kirchhoff's laws after such circuit elements with retardations are given.

2.3 | Circuit equation by Kirchhoff's laws

The circuit equation with the inductance matrix $\boldsymbol{L}$ and potential coefficient matrix $\boldsymbol{P}$ of N inductive elements and M capacitive elements, respectively is formulated as follows: We assume that each inductive element is terminated by the capacitive elements, as shown in Figure 3. Then, we set nodes on the capacitive elements and define $M \times (N+M)$ incidence matrix $\boldsymbol{U}$ as

$$\boldsymbol{U} = [\boldsymbol{U}_\mathrm{l}, \boldsymbol{1}_\mathrm{t}], \tag{8}$$

where $\boldsymbol{U}_\mathrm{l}$ is the incidence matrix of the inductive elements and $\boldsymbol{1}_\mathrm{t}$ is the unit matrix which corresponds to the capacitive elements. For example, the incidence matrix of the structure in Figure 2 is

$$\boldsymbol{U} = \begin{bmatrix} 1 & 0 & 1 & 0 & 0 & 0 \\ -1 & 0 & 0 & 1 & 0 & 0 \\ 0 & 1 & 0 & 0 & 1 & 0 \\ 0 & -1 & 0 & 0 & 0 & 1 \end{bmatrix} \tag{9}$$

We define the $N+M$ branch voltages $\boldsymbol{V}$ by the N branch voltages $\boldsymbol{V}_\mathrm{l}$ of the wires and M node potentials $\widehat{\boldsymbol{V}}$ of the spheres as

$$\boldsymbol{V} \equiv \begin{bmatrix} \boldsymbol{V}_\mathrm{l} \\ \widehat{\boldsymbol{V}} \end{bmatrix} \tag{10}$$

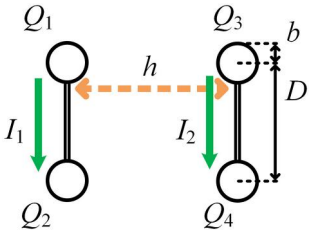

FIGURE 2 Structure of coupled two meta-atoms in parallel position, which has two resonators with retarded coupling. We use parameters of wire radii $a = 0.01$ mm, $b = 1$ mm and $D = 7$ mm in this study

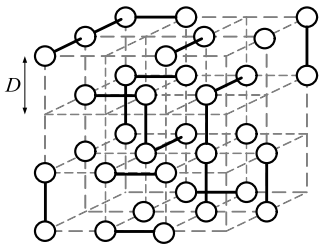

FIGURE 3 Resonator structures with all wires terminated by spheres [22]

We assume that the external excitation $\boldsymbol{V}_{\mathrm{l}}^{\mathrm{E}}$ is applied to the wires and define the $N+M$ voltage source vector $\boldsymbol{V}^{\mathrm{E}}$ as

$$\boldsymbol{V}^{\mathrm{E}} \equiv \begin{bmatrix} \boldsymbol{V}_{\mathrm{l}}^{\mathrm{E}} \\ \boldsymbol{0} \end{bmatrix} \tag{11}$$

Then, we use the Kirchhoff's voltage law to show the existence of the node voltages represented as

$$\boldsymbol{U}^{\mathrm{T}}\widehat{\boldsymbol{V}} = \boldsymbol{V} + \boldsymbol{V}^{\mathrm{E}}, \tag{12}$$

where 'T' indicates the transpose matrix. We define the $N+M$ branch currents $\boldsymbol{I}$ by the N branch currents $\boldsymbol{I}_{\mathrm{l}}$ of wires and M branch currents $\boldsymbol{I}_{\mathrm{t}} = \mathrm{j}\omega\boldsymbol{Q}$ of spheres as

$$\boldsymbol{I} \equiv \begin{bmatrix} \boldsymbol{I}_{\mathrm{l}} \\ \mathrm{j}\omega\boldsymbol{Q} \end{bmatrix} \tag{13}$$

Then, the Kirchhoff's current law can be represented as

$$\boldsymbol{U}\boldsymbol{I} = \boldsymbol{0}. \tag{14}$$

The relationship between the branch voltages $\boldsymbol{V}$ and currents $\boldsymbol{I}$ is given as

$$\boldsymbol{V} = \begin{bmatrix} \mathrm{j}\omega\boldsymbol{L} & \boldsymbol{0} \\ \boldsymbol{0} & \boldsymbol{P}/\mathrm{j}\omega \end{bmatrix} \boldsymbol{I}. \tag{15}$$

From Equations (12), (14), and (15), the equation of the wire currents $\boldsymbol{I}_{\mathrm{l}}$ is given as

$$\left(\mathrm{j}\omega\boldsymbol{L} + \frac{\boldsymbol{U}_{\mathrm{l}}^{\mathrm{T}}\boldsymbol{P}\boldsymbol{U}_{\mathrm{l}}}{\mathrm{j}\omega}\right)\boldsymbol{I}_{\mathrm{l}} = -\boldsymbol{V}_{\mathrm{l}}^{\mathrm{E}}. \tag{16}$$

Since the coefficient matrix of $\boldsymbol{I}_{\mathrm{l}}$ is an impedance matrix and describes the properties of the circuits, we can derive the characteristics of the circuits using the impedance matrix.

2.4 | Power balance by Tellegen's theorem

Because the circuit equation are formulated by Kirchhoff's law, the power balances of complex powers in circuits are given by Tellegen's theorem [26], which are derived using Kirchhoff's laws Equations (12) and (14) as follows.

$$(\boldsymbol{V}+\boldsymbol{V}^{\mathrm{E}})^{\mathrm{T}}\bar{\boldsymbol{I}} = (\boldsymbol{U}^{\mathrm{T}}\widehat{\boldsymbol{V}})^{\mathrm{T}}\bar{\boldsymbol{I}} = \widehat{\boldsymbol{V}}^{\mathrm{T}}\boldsymbol{U}\boldsymbol{I} = 0. \tag{17}$$

where bar represents the complex conjugate. If we use the inductive currents $\boldsymbol{I}_{\mathrm{l}}$ and capacitive currents $\boldsymbol{I}_{\mathrm{t}} = \mathrm{j}\omega\boldsymbol{Q}$, the relation is

$$\mathrm{j}\omega\boldsymbol{I}_{\mathrm{l}}^{\mathrm{T}}\boldsymbol{L}\bar{\boldsymbol{I}}_{\mathrm{l}} + \frac{1}{\mathrm{j}\omega}\boldsymbol{I}_{\mathrm{t}}^{\mathrm{T}}\boldsymbol{P}\bar{\boldsymbol{I}}_{\mathrm{t}} + (\boldsymbol{V}_{\mathrm{l}}^{\mathrm{E}})^{\mathrm{T}}\bar{\boldsymbol{I}}_{\mathrm{l}} = 0. \tag{18}$$

This equation defines the contribution of each element in the power balance. The imaginary parts of $\boldsymbol{L}$ and $\boldsymbol{P}$ generate the real parts of the complex powers which correspond to the radiation loss. The coefficients $\mathrm{j}\omega$ and $1/\mathrm{j}\omega$ of the first and second terms, respectively, give the essential difference contributing to the loss.

3 | RADIATION LOSS

To clarify the property of the radiation loss in circuits, we review the behaviour of the resonator in Figure 1 by the circuit approach. The equivalent circuit Equation (16) of the resonator is given as:

$$Z_{\mathrm{s}}I = -V^{\mathrm{E}} \tag{19}$$

$$Z_{\mathrm{s}}(\omega) \equiv \mathrm{j}\omega L_{\mathrm{s}}(\omega) + \frac{1}{\mathrm{j}\omega}P_{\mathrm{s}}(\omega) \tag{20}$$

$$P_{\mathrm{s}}(\omega) \equiv P_{\mathrm{s1}}(\omega) - P_{\mathrm{s2}}(\omega), \tag{21}$$

$$P_{\mathrm{s1}}(\omega) \equiv \frac{\exp\left(-\mathrm{j}\omega\frac{b}{c}\right)}{2\pi\varepsilon_0 b},\ P_{\mathrm{s2}}(\omega) \equiv \frac{\exp\left(-\mathrm{j}\omega\frac{D}{c}\right)}{2\pi\varepsilon_0 D}. \tag{22}$$

If we set $a = 0.01$ mm, $b = 1$ mm and $D = 7$ mm in Figure 1, the real and imaginary parts of the frequency characteristics of the impedance Z_{s} are shown in Figures 4 and 5, respectively. Because the loss is caused by retardation, the Re $[Z_{\mathrm{s}}]$ without retardation (dotted line) equals 0 in Figure 4, where Re[·] denotes the real part of '·'. The ω^* satisfying Im $[Z_{\mathrm{s}}(\omega^*)] = 0$ in Figure 5 is the resonant angular frequency since the real impedance Z_{s} means resonance, where Im[·] is the imaginary part of '·'.

To clarify the meaning of the loss caused by the impedance Z_{s} with the retardation, we show the phase relation of the

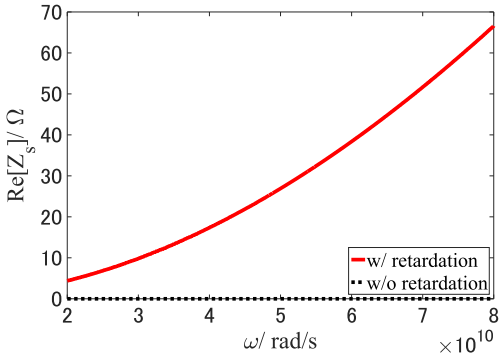

FIGURE 4 Frequency characteristics of impedance Z_{s} (real part) with and without retardation. Since the loss is caused by retardation, the real part without retardation is equal to 0

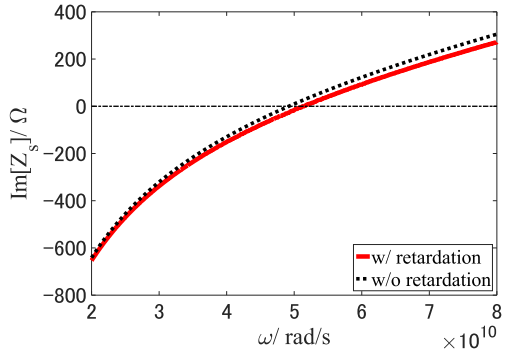

FIGURE 5 Frequency characteristics of impedance Z_s (imaginary part) with and without retardation

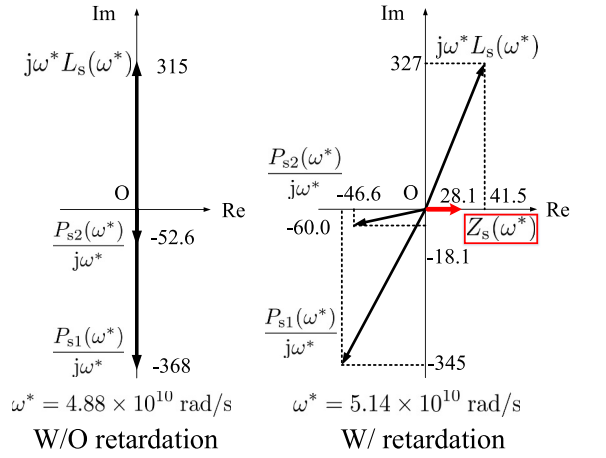

FIGURE 6 Phase relation among impedances. W/O retardation: L_s, P_s are real numbers; hence, Z_s is an imaginary number. W/ retardation: L_s, P_s are complex numbers; hence, Z_s is a complex number

impedances in a complex plane at the resonant frequency ω^* in Figure 6. Although the impedance has only the imaginary components in the case without retardation, $j\omega^* L_s$ and $P_{s1}/j\omega^*$, $P_{s2}/j\omega^*$ rotate on a complex plane because of the retardation factors and they become complex numbers. The real parts of the capacitive elements are negative; however, the total real part $\mathrm{Re}[j\omega^* L_s + (P_{s1} - P_{s2})/j\omega^*]$ becomes positive because of the inductive element.

The second order Taylor polynomials of the impedances [23] are

$$\mathrm{Re}\left[j\omega L_s(\omega)\right] = \frac{\mu_0}{4\pi}\frac{D^2}{c}\omega^2 \tag{23}$$

$$\mathrm{Re}\left[\frac{1}{j\omega}P_s(\omega)\right] = -\frac{1}{3}\left(\frac{\mu_0}{4\pi}\frac{D^2+b^2}{c}\omega^2\right) \tag{24}$$

The real part of the capacitive impedance Equation (24) is negative. When $b \ll D$ is satisfied, one-third of the real part by the inductive elements is cancelled by the capacitive elements. The total real parts of the impedance agrees with

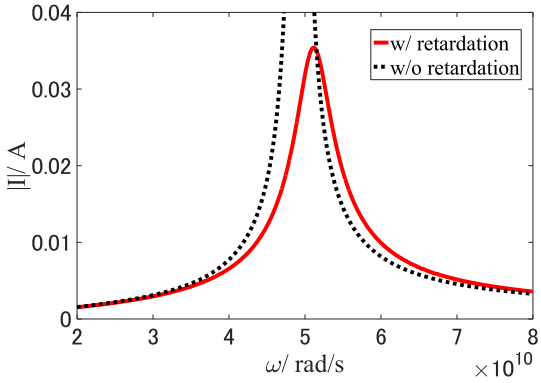

FIGURE 7 Frequency characteristics of current I in Figure 1 with $V^E = 1$

the radiation resistance by a small dipole [7]. Figure 7 shows the frequency characteristics of the current $|I|$ when $V^E = 1$. Although the frequency characteristics without retardation approach infinity at the resonant frequency, the case with retardation is finite and the value of the current is confirmed based on the electromagnetic analysis in [23]. Thus, the total contributions of the positive [Equation (23)] and negative [Equation (24)] real parts give the radiation loss in the circuits. The power balance [Equation (18)] in this case is written by

$$j\omega L_s|I|^2 + \frac{P_{s1} - P_{s2}}{j\omega}|I|^2 + V^E\bar{I} = 0.$$

At the resonant angular frequency ω^*, the V^E and I are in phase, and the supplied complex power $V^E\bar{I}$ is real. The real part of the inductive and capacitive parts is $41.5\ |I|^2$ and $(-\ 60.0\ +\ 46.6)|I|^2$ in Figure 6, respectively. If we substitute the current value $I = 0.0356$ in Figure 7, we can confirm that the balance is satisfied.

4 | RETARDED COUPLING

4.1 | Resonant angular frequencies of two modes

To clarify the property of the retarded coupling, we review the behaviour of the coupled resonators in Figure 2 by circuit analysis. The circuit Equation (16) of the structure is given as

$$\left(j\omega\boldsymbol{L}(\omega) + \frac{1}{j\omega}\boldsymbol{U}_1^{\mathrm{T}}\boldsymbol{P}\boldsymbol{U}_1(\omega)\right)\begin{bmatrix} I_1 \\ I_2 \end{bmatrix} = -\begin{bmatrix} 0 \\ 0 \end{bmatrix} \tag{25}$$

$$\boldsymbol{L}(\omega) = \begin{bmatrix} L_s & L_m \\ L_m & L_s \end{bmatrix}, \quad \boldsymbol{U}_1^{\mathrm{T}}\boldsymbol{P}\boldsymbol{U}_1(\omega) = \begin{bmatrix} P_s & P_m \\ P_m & P_s \end{bmatrix}, \tag{26}$$

where $L_m \equiv L_{12}$ in Equation (4) and P_m is defined as

$$P_{\mathrm{m}}(\omega) \equiv \frac{1}{2\pi\varepsilon_0}\left(\frac{\exp\left(-\mathrm{j}\omega\frac{h}{c}\right)}{h} - \frac{\exp\left(-\mathrm{j}\omega\frac{\sqrt{D^2+h^2}}{c}\right)}{\sqrt{D^2+h^2}}P\right) \tag{27}$$

Using the symmetry in Equation (25), we decompose the equation into even and odd modes as

$$\begin{bmatrix} \mathrm{Z_s}+\mathrm{Z_m} & 0 \\ 0 & \mathrm{Z_s}-\mathrm{Z_m} \end{bmatrix}\begin{bmatrix} I_1+I_2 \\ I_1-I_2 \end{bmatrix} = \begin{bmatrix} 0 \\ 0 \end{bmatrix}, \tag{28}$$

where

$$\mathrm{Z_s}(\omega) \equiv \mathrm{j}\omega L_{\mathrm{s}}(\omega) + \frac{P_{\mathrm{s}}(\omega)}{\mathrm{j}\omega}, \tag{29}$$

$$\mathrm{Z_m}(\omega) \equiv \mathrm{j}\omega L_{\mathrm{m}}(\omega) + \frac{P_{\mathrm{m}}(\omega)}{\mathrm{j}\omega}. \tag{30}$$

If we define mode-impedances of even and odd modes as

$$\tilde{\mathrm{Z}}_{\mathrm{e}}(\omega) \equiv \mathrm{Z_s}+\mathrm{Z_m}, \quad \tilde{\mathrm{Z}}_{\mathrm{o}}(\omega) \equiv \mathrm{Z_s}-\mathrm{Z_m}, \tag{31}$$

then the resonant angular frequencies ω_{e}^* and ω_{o}^* are given by the imaginary part of the impedances

$$\mathrm{Im}[\tilde{\mathrm{Z}}_{\mathrm{e}}(\omega)] = 0, \quad \mathrm{Im}[\tilde{\mathrm{Z}}_{\mathrm{o}}(\omega)] = 0, \tag{32}$$

respectively.

The distance h dependencies of ω_{e}^* and ω_{o}^* are shown in Figure 8. The period of the cross points of the ω_{e}^* and ω_{o}^* is approximately half of the wavelength $\lambda = 2\pi c/\omega^* = 36.7$ mm. In contrast, the radiation losses $\mathrm{Re}[\tilde{\mathrm{Z}}_{\mathrm{e}}(\omega_{\mathrm{e}}^*)]$ and $\mathrm{Re}[\tilde{\mathrm{Z}}_{\mathrm{o}}(\omega_{\mathrm{o}}^*)]$ shown in Figure 9 also have a similar period, and the cross points in Figure 8 correspond to the maximal or minimum points in Figure 9. That is, the cross points in Figure 8 satisfy $\mathrm{Im}[\mathrm{Z_m}(\omega_{\mathrm{e}}^*)] = \mathrm{Im}[\mathrm{Z_m}(\omega_{\mathrm{o}}^*)] = 0$ as in Equation (31) and at these points the real parts $\mathrm{Re}[\mathrm{Z_m}(\omega_{\mathrm{e}}^*)]$ and $\mathrm{Re}[\mathrm{Z_m}(\omega_{\mathrm{o}}^*)]$ become maximum or minimum, as shown in Figure 9. Such a relation was also confirmed by the electromagnetic simulations and natural frequencies in [23].

4.2 | Resonant frequency and loss by retarded coupling

To understand the relation between the resonant angular frequency and loss, we estimate the mutual impedance $\mathrm{Z_m}$ in Equation (30) under the condition of $D \ll h$. The mutual inductance $L_{\mathrm{m}} = L_{12}$ in Equation (4) is approximated by L_{12} in Equation (5) and has the factor $\frac{1}{h}e^{-\mathrm{j}\omega\frac{h}{c}}$. Similarly, P_{m} in Equation (27) is approximated by

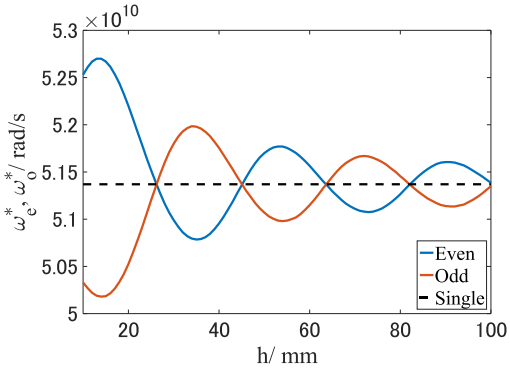

FIGURE 8 Distance h dependencies of resonant angular frequencies ω_{e}^* and ω_{o}^*

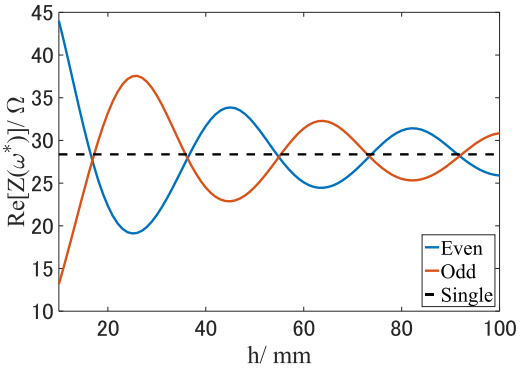

FIGURE 9 Distance h dependencies of the radiation losses $\mathrm{Re}[\tilde{\mathrm{Z}}_{\mathrm{e}}(\omega_{\mathrm{e}}^*)]$ and $\mathrm{Re}[\tilde{\mathrm{Z}}_{\mathrm{o}}(\omega_{\mathrm{o}}^*)]$ on the resonant angular frequency

$$P_{\mathrm{m}} \sim \mathrm{j}\frac{\omega D^2}{4\pi\varepsilon_0 c h^2}\exp\left(-\mathrm{j}\omega\frac{h}{c}\right), \tag{33}$$

and has the factor $\frac{1}{h^2}e^{-\mathrm{j}\omega\frac{h}{c}}$. Because the inductive elements are dominant, $\mathrm{Z_m}$ defined by Equation (30) is approximated as

$$\mathrm{Z_m}(\omega) \sim \mathrm{j}\omega\frac{\mu_0}{4\pi}\frac{D^2}{h}\exp\left(-\mathrm{j}\omega\frac{h}{c}\right) \tag{34}$$

Thus, the circuit Equation (28) is expressed as the following approximation,

$$\left[\mathrm{Z_s} + \mathrm{j}\omega\frac{\mu_0}{4\pi}\frac{D^2}{h}\exp\left(-\mathrm{j}\omega\frac{h}{c}\right)\right]\tilde{I}_{\mathrm{e}} = 0 \tag{35}$$

$$\left[\mathrm{Z_s} - \mathrm{j}\omega\frac{\mu_0}{4\pi}\frac{D^2}{h}\exp\left(-\mathrm{j}\omega\frac{h}{c}\right)\right]\tilde{I}_{\mathrm{o}} = 0, \tag{36}$$

where $\tilde{I}_{\mathrm{e}} \equiv I_1 + I_2$ and $\tilde{I}_{\mathrm{o}} \equiv I_1 - I_2$.

Figure 10 shows the original Equation (30) and approximated Equation (34) and $\mathrm{Z_m}$ on a complex plane with the parameter h. Thus, the phase of the retarded factor rotates the mutual impedance depending on the distance between meta-atoms h and contributes to the relationship between the resonant frequency and loss in Figures 8 and 9. That is, when Im

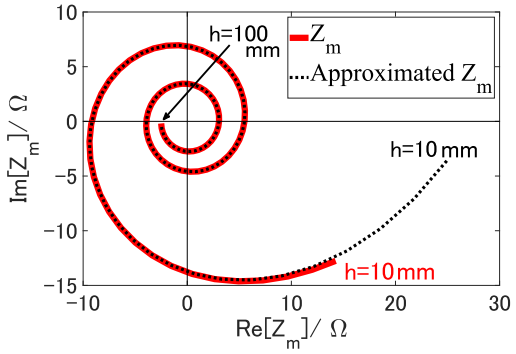

FIGURE 10 Comparison of mutual impedance Z_m between Equations (30) and (34): changing h at $\omega^* = 5.14 \times 10^{10}$ rad/s. The mutual impedance rotates in a complex plane depending on h and generates the relation between the resonant frequency and radiation loss

$[Z_m(\omega^*)] = 0$ is satisfied because Equations (35) and (36), ω_e^* is equal to ω_o^* in Figure 8 and the large real parts $|\mathrm{Re}[Z_m(\omega_e^*)]|$ and $|\mathrm{Re}[Z_m(\omega_o^*)]|$ causes the maximum or minimum radiation loss in Figure 9.

4.3 | Comparison with delay in transmission line

To clarify the property of the retarded coupling, we compare the retarded coupling of resonators in Figure 2 with coupling through conducting wires of a transmission line shown in Figure 11. The difference between the retarded coupling and the coupling through the conducting wire is well known in the discussion of electromagnetic fields. However, it is important to clarify the essential difference of circuit elements that contain delays. In this discussion, we assume that the transmission line has no losses and its characteristic impedance, propagation constant, and length are Z_0, $\mathrm{j}\beta$, and h, respectively. We define the lumped circuit parameters as follows:

$$L = \mathrm{Re}[L_s(\omega^*)],\quad C = \mathrm{Re}\left[\frac{1}{P_s(\omega^*)}\right],\quad R = \mathrm{Re}[Z_s(\omega^*)], \tag{37}$$

where ω^* is the resonant angular frequency of Figure 1.

The lumped circuit equation of each resonator is expressed as

$$\left(\mathrm{j}\omega L + \frac{1}{\mathrm{j}\omega C} + R\right) I_1 = -V_1 \tag{38}$$

$$\left(\mathrm{j}\omega L + \frac{1}{\mathrm{j}\omega C} + R\right) I_2 = V_2. \tag{39}$$

The coupling by the transmission line is

$$\begin{bmatrix} V_1 \\ I_1 \end{bmatrix} = \boldsymbol{F}\begin{bmatrix} V_2 \\ I_2 \end{bmatrix},\quad \boldsymbol{F} \equiv \begin{bmatrix} \cos\beta h & \mathrm{j}Z_0 \sin\beta h \\ \dfrac{\mathrm{j}}{Z_0}\sin\beta h & \cos\beta h \end{bmatrix} \tag{40}$$

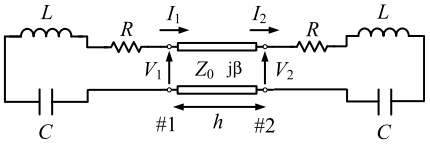

FIGURE 11 Two resonators coupled by a lossless transmission line

If we decompose Equations (38) and (39) into two current modes in the same way as the retarded couplings,

$$\tilde{I}_e = I_1 + (-I_2),\quad \tilde{I}_o = I_1 - (-I_2), \tag{41}$$

the circuit equation of each eigenmode is expressed by

$$\left(Z_{s'} - \mathrm{j}\frac{Z_0}{\sin\left(\omega\frac{h}{c}\right)}\right)\tilde{I}_e = 0, \tag{42}$$

$$\left(Z_{s'} + \mathrm{j}\frac{Z_0}{\sin\left(\omega\frac{h}{c}\right)}\right)\tilde{I}_o = 0, \tag{43}$$

where we set $\beta = \frac{\omega}{c}$ and

$$Z_{s'} = \mathrm{j}\omega L + \frac{1}{\mathrm{j}\omega C} + R - \mathrm{j}\frac{Z_0}{\tan\left(\omega\frac{h}{c}\right)}. \tag{44}$$

Because Equations (42) and (43) correspond to Equations (35) and (36), respectively, the impedance Z_m in Equation (34) is replaced by

$$Z_{m'} = -\mathrm{j}\frac{Z_0}{\sin\left(\omega\frac{h}{c}\right)}. \tag{45}$$

Although the mutual impedance Z_m rotates in the complex plane, depending on h (shown in Figure 10), $Z_{m'}$ for the transmission line is always a pure imaginary number depending on h (shown in Figure 12) and does not exhibit coupling loss. Thus, the couplings in Figures 2 and 11 are essentially different with regard to the energy loss and the retarded coupling provides new elements in the circuit analysis.

5 | RADIATION REACTIONS IN ARRAY OF META-ATOMS

5.1 | Dispersion characteristics with retardation

As an example of where the retarded coupling plays an essential role, this section addresses the radiation reactions in the 1D array structure of meta-atoms shown in Figure 13. Relationships

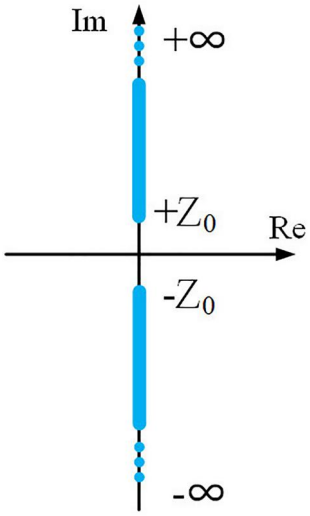

FIGURE 12 Mutual impedance $Z_{m'}$ in the circuit by transmission line. The mutual impedance is a pure imaginary number dependent on h. Although the coupling caused by a lossless transmission line has retardation, the coupling does not generate loss

between the propagation modes and resonant frequencies are represented by the dispersion characteristics, and these properties are often used in the design of metamaterials. We show the singularity on a dispersion curve [7] created by the retarded coupling theoretically using circuit analysis.

To derive the dispersion curve, we introduce the periodic boundary condition, such that $\boldsymbol{L}$ and $\boldsymbol{U}_1^{\mathrm{T}}\boldsymbol{P}\boldsymbol{U}_1$ become circulant matrices. Then, the impedance matrix $\boldsymbol{Z}$ is also a circulant matrix,

$$\boldsymbol{Z}(\omega)=\begin{bmatrix} Z_0 & Z_1+Z_{N-1} & \cdots & Z_1+Z_{N-1} \\ Z_1+Z_{N-1} & Z_0 & \ddots & Z_2+Z_{N-2} \\ \vdots & \ddots & \ddots & \vdots \\ Z_1+Z_{N-1} & Z_2+Z_{N-2} & \cdots & Z_0 \end{bmatrix}, \tag{46}$$

where $Z_0 = Z_s$ and Z_n ($n = 1, 2, \ldots, N-1$) is defined by

$$Z_n = \mathrm{j}\omega L_n + \frac{P_n}{\mathrm{j}\omega}, \tag{47}$$

$$L_n \equiv \frac{\mu_0 D}{2\pi}\left(\ln\left(\frac{\eta}{n}+\sqrt{1+\frac{\eta^2}{n^2}}\right)-\sqrt{1+\frac{n^2}{\eta^2}}+\frac{n}{\eta}\right)e^{-\mathrm{j}\omega\frac{nb}{c}},$$

$$P_n \equiv \frac{1}{2\pi\varepsilon_0}\left(\frac{\exp\left(-\mathrm{j}\omega\frac{nh}{c}\right)}{nh}-\frac{\exp\left(-\mathrm{j}\omega\frac{\sqrt{D^2+(nh)^2}}{c}\right)}{\sqrt{D^2+(nh)^2}}\right), \tag{48}$$

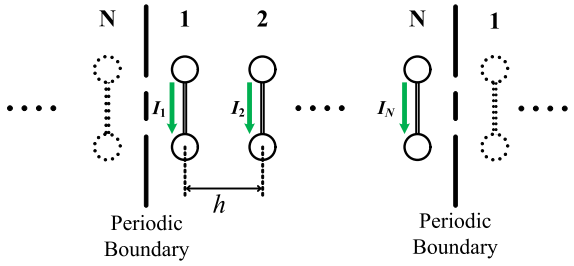

FIGURE 13 1D array structure of the meta-atoms. Each meta-atom is a resonator in Figure 1

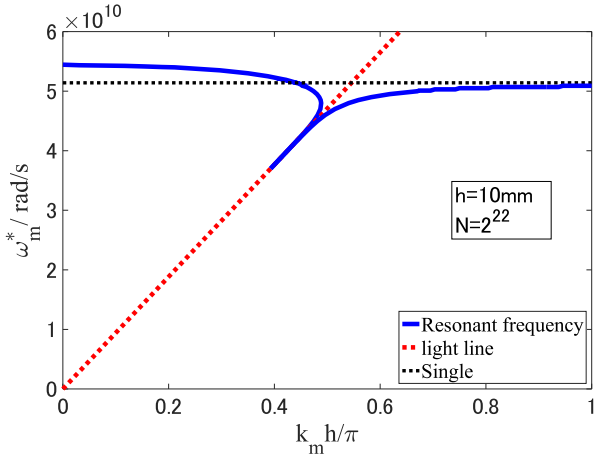

FIGURE 14 Dispersion characteristics of 1D array structure (Figure 13). The curve has a singularity on the light line. 'Single' is the resonant frequency of the single meta-atom

The circulant matrix (46) is diagonalised by a discrete Fourier transform (DFT) matrix, whose column vectors are written by

$$\left[1,\ e^{\mathrm{j}2\pi\frac{m}{N}},\ e^{\mathrm{j}2\pi\frac{2m}{N}},\ \ldots,\ e^{\mathrm{j}2\pi\frac{(N-1)m}{N}}\right]^{\mathrm{T}} \quad (m=0,\ 1,\ 2,\ \ldots,\ N-1). \tag{49}$$

The mth eigenvector corresponds to the wave number of mth eigenmode and is expressed as $k_m = \frac{2\pi m}{Nh}$. Using the eigenvectors in Equation (49), we derive the eigenvalue, that is, the mth mode impedance as

$$\tilde{Z}(\omega, k_m) = Z_0 + \sum_{n=1}^{N-1}(Z_n + Z_{N-n})e^{\mathrm{j}2\pi\frac{nm}{N}}. \tag{50}$$

Solving the equation of ω yields the resonant condition of the mth mode,

$$\mathrm{Im}[\tilde{Z}(\omega, k_m)] = 0, \tag{51}$$

we obtain the resonant angular frequency ω_m^* and real part of the impedance, which represent the radiation loss in the resonant angular frequency of each wave number k_m. The dispersion

characteristics $(k_m,\ \omega_m^*)$ and real parts $(k_m,\ \mathrm{Re}[\tilde{Z}(\omega_m^*, k_m)])$ are shown in Figures 14 and 15. The dispersion curve has a singularity on the light line and the real part of mode impedances changes discontinuously on the light line. This property is well known as the fact that the Bloch mode is no longer fully guided after crossing the light line [27]; however, the property is not described by circuit analysis without retardation.

To discuss the relation between Figures 14 and 15, we show the real and imaginary parts of the mode impedance $\tilde{Z}(\omega, k_m)$ in Figures 16 and 17, respectively. The cross point of the plane $\mathrm{Im}[\tilde{Z}] = 0$ in Figure 17 corresponds to the dispersion curve in Figure 14, while the real parts $\mathrm{Re}[\tilde{Z}(\omega_m^*, k_m)]$ on the curve in Figure 16 represent the curves in Figure 15. The discontinuity in Figure 15 corresponds to the discontinuity on the light line in Figure 16. Thus, the radiation loss and resonant frequency are represented by the real and imaginary parts of the mode impedance $\tilde{Z}(\omega, k_m)$.

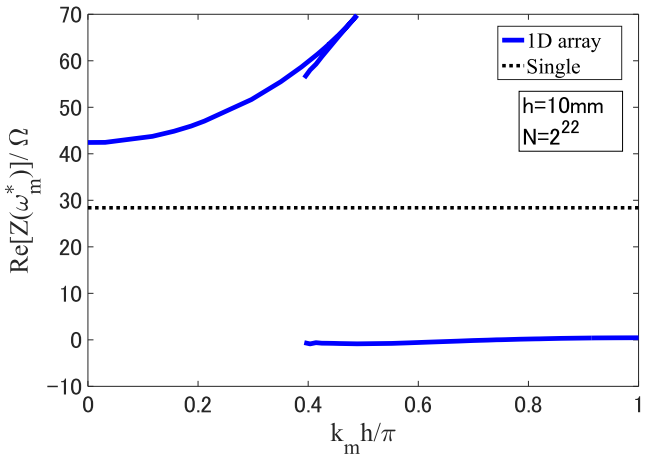

FIGURE 15 Real part of mode impedance on the resonant angular frequency. The curve has a discontinuity where the dispersion curve crosses the light line. 'Single' is the real part of the single meta-atom

5.2 | Analytical estimation of radiation loss

To derive the analytical estimation of the radiation loss by circuit analysis, we divide the contributions of the inductances and potential coefficients in the real part of the mode impedance as follows:

$$\mathrm{Re}[\tilde{Z}(\omega, k_m)] = \mathrm{Re}[\tilde{Z}_{\mathrm{L}}(\omega, k_m)] + \mathrm{Re}[\tilde{Z}_{\mathrm{P}}(\omega, k_m)]. \tag{52}$$

Furthermore, approximating Equation (5), we define the imaginary part of the inductance L_n^{i} $(n = 0, 1, \ldots, N-1)$ as

$$L_n^{\mathrm{i}} \equiv -\frac{\mu_0 D^2 \omega}{4\pi c} \frac{\sin\left(\omega \frac{nh}{c}\right)}{\omega \frac{nh}{c}} \tag{53}$$

which is a Sinc function and is caused by retarded couplings. Then, the contribution of the inductance $\mathrm{Re}[\tilde{Z}_{\mathrm{L}}(\omega, k_m)]$ can be written by

$$\mathrm{Re}[\tilde{Z}_{\mathrm{L}}(\omega, k_m)] = -\omega L_0^{\mathrm{i}} + \sum_{n=1}^{N-1} -\omega (L_n^{\mathrm{i}} + L_{N-n}^{\mathrm{i}}) e^{2\pi \frac{nm}{N}}, \tag{54}$$

$$= \frac{\mu_0 D^2 \omega^2}{4\pi c} \sum_{n=-(N-1)}^{N-1} \frac{\sin\left(\omega \frac{nh}{c}\right)}{\omega \frac{nh}{c}} \cos\left(2\pi \frac{nm}{N}\right)$$

$$\simeq \begin{cases} \frac{\mu_0 D^2 \omega}{4h} & (ck_m < \omega) \\ \frac{\mu_0 D^2 \omega}{8h} & (ck_m = \omega) \\ 0 & (ck_m > \omega) \end{cases}, \tag{55}$$

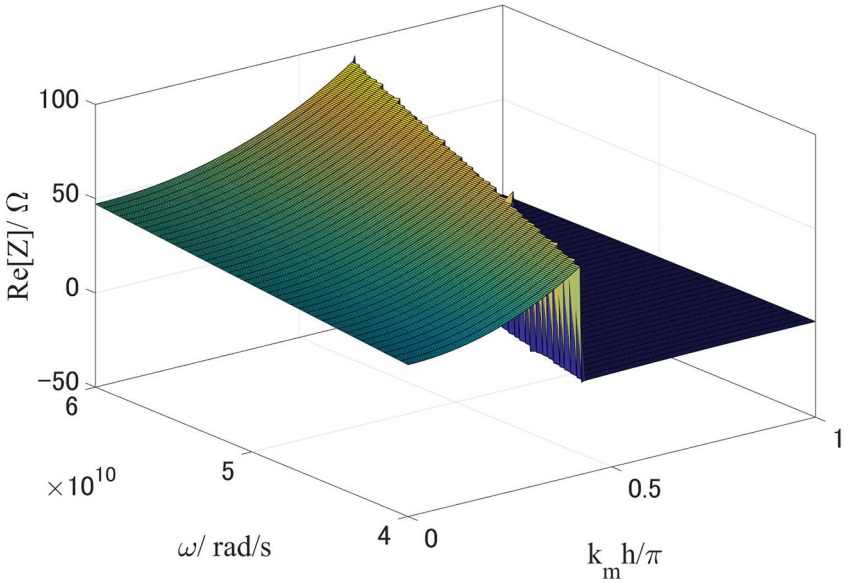

FIGURE 16 Real part of mode impedance (Re $[\tilde{Z}(\omega, k_m)]$). The impedance has a discontinuity on the light line

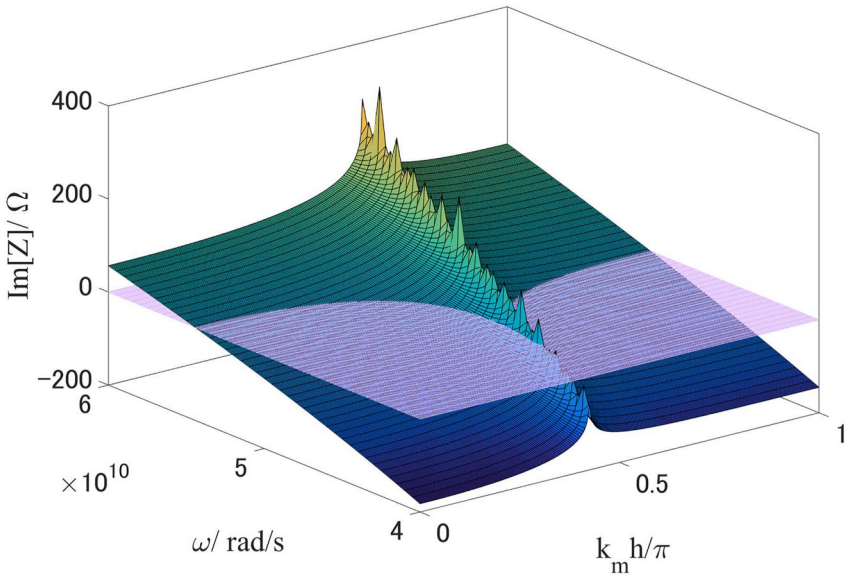

FIGURE 17 Imaginary part of mode impedance ($\mathrm{Im}[\tilde{Z}(\omega, k_m)]$): the cross point of the plane $\mathrm{Im}[\tilde{Z}] = 0$ corresponds to the dispersion curve in Figure 14

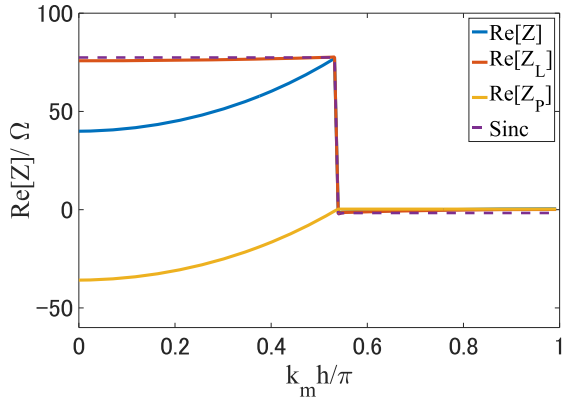

FIGURE 18 Components in Equation (52) at $\omega = 5.14 \times 10^{10}$ (rad/s). The inductance loss is approximated as a Sinc function and generates radiation loss discontinuity

which is a window function when N is significantly large. Thus, the discontinuity of $\mathrm{Re}[\tilde{Z}_L(\omega, k_m)]$ on the light line is shown analytically by the circuit model.

The potential coefficient Equation (48) also consists of the Sinc function; however, the second term has irregular samp ling. The contributions of $\mathrm{Re}[\tilde{Z}(\omega, k_m)]$, $\mathrm{Re}[\tilde{Z}_L(\omega, k_m)]$, $\mathrm{Re}[\tilde{Z}_P(\omega, k_m)]$ at $\omega = 5.14 \times 10^{10}$ are shown in Figure 18. We can confirm that $\mathrm{Re}[\tilde{Z}_L(\omega, k_m)]$ is approximated by the Sinc function and discontinuity in $\mathrm{Re}[\tilde{Z}(\omega, k_m)]$ is caused by inductive couplings. The retarded inductive couplings generate the radiation loss discontinuity on the light line which is an important characteristic of radiation by leaky-waves [28].

6 | CONCLUSION

We introduced a circuit with retarded couplings to describe the radiation loss resulting from a radiation reaction.

The potential coefficient matrix was used instead of the capacitance matrix because of the retardation. The circuit equations were formulated such that the real parts of the complex power with the retarded couplings describe the radiation loss. Using the simple resonant circuit, we initially demonstrated the radiation loss mechanism by the retardation of the inductance and potential coefficients to clarify the contribution of the inductive and capacitive elements. We then clarified the radiation reaction in the coupled resonant circuit. The relation between radiation loss and resonant frequency was shown by the phase rotation of the retarded coupling. We discussed the essential difference between the retarded coupling and the coupling with the transmission line. We then analysed the 1D array of resonators with all retarded couplings. The radiation loss was discontinuously changed on the light line and the dispersion curve has singularity on the light line. Thus, the circuit with the retarded coupling describes the radiation reaction and generates novel characteristics that are not described by the circuit without retardation. The circuit analysis of the radiation reaction will afford new aspects in studies on topics such as metamaterials and plasmonics.

ACKNOWLEDGEMENT

This research study was supported in part by Grants-in-Aid for Scientific Research (Grant Nos. 18K04139 and 15K06063).

CONFLICT OF INTEREST

None.

DATA AVAILABILITY STATEMENT

Data are openly available in a public repository that issues datasets with DOIs.

ORCID

Takashi Hisakado https://orcid.org/0000-0002-5078-2296

REFERENCES

1. Engheta, N.: Circuits with light at nanoscales: optical nanocircuits inspired by metamaterials. Science. 317, 1698–1702 (2007)
2. Caloz, C., Itoh, T.: Electromagnetic Metamaterials. Wiley, New York (2006)
3. Rong, C., et al.: A critical review of metamaterial in wireless power transfer system. IET Power Electron. (2021). https://doi.org/10.1049/pel2.12099
4. Bilotti, F., et al.: Equivalent-circuit models for the design of metamaterials based on artificial magnetic inclusions. IEEE Trans. Microw. Theory Tech. 55(12), 2865–2873 (2007)
5. Shamonin, M., et al.: Properties of a metamaterial element: analytical solutions and numerical simulations for a singly split double ring. J. Appl. Phys. 95(7), 3778–3784 (2004)
6. Baena, J.D., et al.: Equivalent-circuit models for split-ring resonators and complementary split-ring resonators coupled to planar transmission lines. IEEE Trans. Microw. Theory Tech. 53(4), 1451–1461 (2005)
7. Solymar, L., Shamonina, E.: Waves in Metamaterials. Chap. 8, pp. 251–287. OXFORD (2009)
8. Alù, A., Maslovski, S.: Power relations and a consistent analytic model for receiving wire antennas. IEEE Trans. Antennas Propag. 58(5), 1436–1448 (2010)
9. Liberal, I., Ziolkowski, R.W.: Analytical and equivalent circuit models to elucidate power balance in scattering problems. IEEE Trans. Antennas Propag. 61(5), 2714–2726 (2013)
10. Rumsey, V.H.: Reaction concept in electromagnetic theory. Phys. Rev. 94(6), 1483–1491 (1954)
11. Heeb, H., Ruehli, A.E.: Three-dimensional interconnect analysis using partial element equivalent circuits. IEEE Trans. Circuits Syst. 39(11), 974–982 (1992)
12. Taubert, R., et al.: Classical analog of electromagnetically induced absorption in plasmonics. Nano Lett. 12, 1367–1371 (2012)
13. Tashiro, D., et al.: Single-Conductor transmission line model incorporating radiation reaction. IEEE Trans. Electromagn. Compat. 63(4), 1065–1077 (2021)
14. Ruehli, A.E.: Interconnection modeling. In: Circuit Analysis, Simulation and Design, pp. 221–253. North-Holland, Amsterdam (1987)
15. Ruehli, A.E., Cangellaris, A.C.: Progress in the methodologies for the electrical modeling of the interconnects and electronic packages. Proc. IEEE. 89(5), 740–771 (2001)
16. Verbeek, M.E.: Partial element equivalent circuit (PEEC) models for on-chip passives and interconnects. Int. J. Numer. Model. 17, 61–84 (2004)
17. Yeung, L.K., Wu, K.-L.: Generalized partial element equivalent circuit (PEEC) modeling with radiation effect. IEEE Trans. Microw. Theory Tech. 59(10), 2377–2384 (2011)
18. Cao, Y.S., et al.: Distributive radiation and transfer characterization based on the PEEC method. IEEE Trans. Electromagn. Compat. 57(4), 734–742 (2015)
19. Ferranti, F., Romano, D., Antonini, G.: On the passivity of the quasi-static partial element equivalent circuit method. Int. J. Circ. Theor. Appl. 47, 304–319 (2018). https://doi.org/10.1002/cta.2588
20. Chou, C., Lee, W., Wu, T.: A rigorous proof on the radiation resistance in generalized PEEC model. IEEE Trans. Microw. Theory Tech. 64(12), 4091–4097 (2016)
21. Dou, Y., Wu, K.: Nature of antenna radiation revealed by physical circuit model. IEEE. Trans. Antenna Propag. 60(1), 84–96 (2021)
22. Hisakado, T., et al.: Equivalent-circuit model for meta-atoms consisting of wired metallic spheres. IEICE Trans. Electron. 100-C(3), 305–312 (2017)
23. Ohishi, K., et al.: Equivalent-circuit model with retarded electromagnetic coupling for meta-atoms of wired metallic spheres. IEICE Trans. Electron. E101-C(12), 923–930 (2018)
24. Zhuromskyy, O., et al.: Slow waves on magnetic metamaterials and on chains of plasmonic nanoparticles: driven solutions in the presence of retardation. J. Appl. Phys. 106, 104908 (2009)
25. Koenderink, A.F., Polman, A.: Complex response and polariton-like dispersion splitting in periodic metal nanoparticle chains. Phys. Rev. B. 74, 033402 (2006)
26. Penfield, P., Spence, R., Duinker, S.: A generalized form of Tellegen's theorem. IEEE Trans. Circuit Theory CT-17(3), 302–305 (1970)
27. Jannopoulos, J.D., Meade, R.D., Winn, J.N.: Photonic Crystals—Molding the Flow of Light. Princeton University Press, Princeton (1995)
28. Kraus, J.D.: ANTENAS, 2nd ed. McGraw Hill Book Co., New York (1988)

How to cite this article: Nakata, R., et al.: Circuit analysis of radiation reaction in metamaterials by retarded electromagnetic coupling. IET Circuits Devices Syst. 16(4), 311–321 (2022). https://doi.org/10.1049/cds2.12104